EUMETSAT POLAR SYSTEM - SECOND GENERATION: PRE-LAUNCH CHARACTERIZATION OF THE MICROWAVE SOUNDER (MWS) ONBOARD METOP-SG A1

Imke Krizek[1], Sabatino Di Michele[1], Jörg Ackermann[1], V. Mattioli[1], M. Labriola[1], D. Schobert[2]

[1]EUMETSAT, Eumetsat Allee 1, 64295 Darmstadt, Germany
[2]ESA-ESTEC, Keplerlaan 1, 2201 AZ Noordwijk, The Netherlands

Email: Jörg.Ackermann@eumetsat.int

25th International TOVS Study Conference
Goa, India, 8-14 May 2025

Abstract

The MicroWave Sounder MWS is a cross-track scanning radiometer, equipped with 24 channels ranging from 23.8 to 229 GHz, designed to provide comprehensive temperature and water vapor soundings in all sky conditions. MWS builds on the legacy of previous instruments from the current EUMETSAT EPS mission, such as the Advanced Microwave Sounding Unit (AMSU) and the Microwave Humidity Sounder (MHS), with improved sensitivity and broader spectral coverage. Notably, it includes a new channel at 229 GHz for improved sensitivity to cloud ice with respect to the 183 GHz measurements.

We present the Metop-SG A1 MWS radiometric performance based on pre-launch RadCal and Antenna campaigns, showing the main calibration parameters that have been derived, to be included in the L1B operational processing.

Microwave Sounder (MWS)

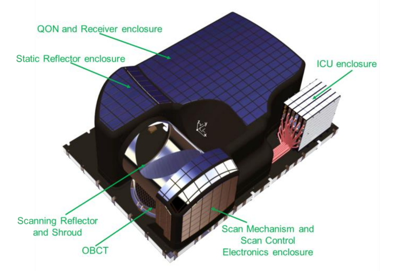

Fig. provided by ESA; in EPS-SG MicroWave Sounder (MWS) Science Plan [1]

- Primary role: Temperature and humidity sounding
- Compact design: combines heritage to both AMSU-A and MHS on board NOAA and Metop satellites
- Total of 24 channels: bands in range 23-229 GHz
- Cross-track scanner

1. Radiometric characterization & calibration

Radiometric Calibration Campaign: Setup

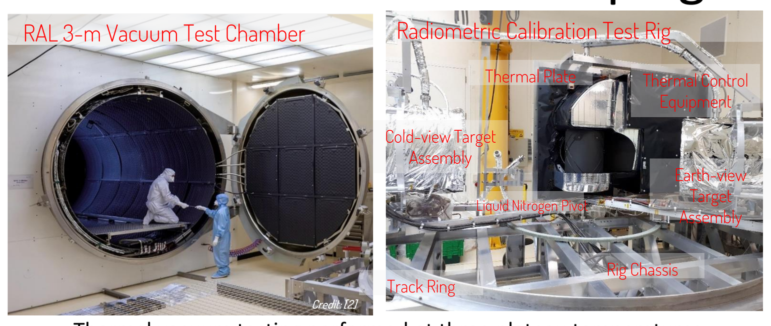

Thermal vacuum testing performed at three plateau temperatures

Predicted temperatures for each Plateau (in °C)				
Plateau	STC Shroud (Chamber Wall)	Instrument Baseplate Interface	ICU plate	Instrument Shroud (Control Plates)
T1	-40	-25	-20	(-20)*
T2	-40	0	0	0
T3	-40	20	15	15

(*) In PFM campaign, only a value warmer than -20 was achieved

1.1 Radiometric sensitivity

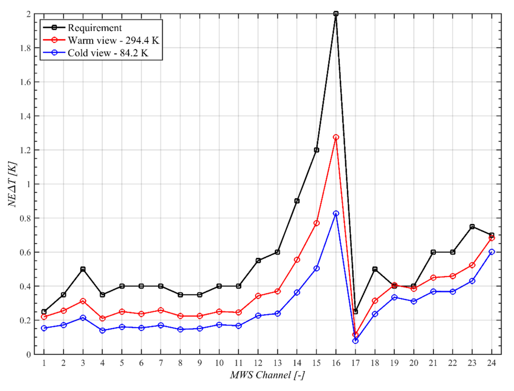

- NEΔT per channel for warm view (at 294.4 K), cold view (at 84.2 K) and requirement
- Power spectral density (PSD) plots of warm target view counts (in pointing mode) shown in the plot below

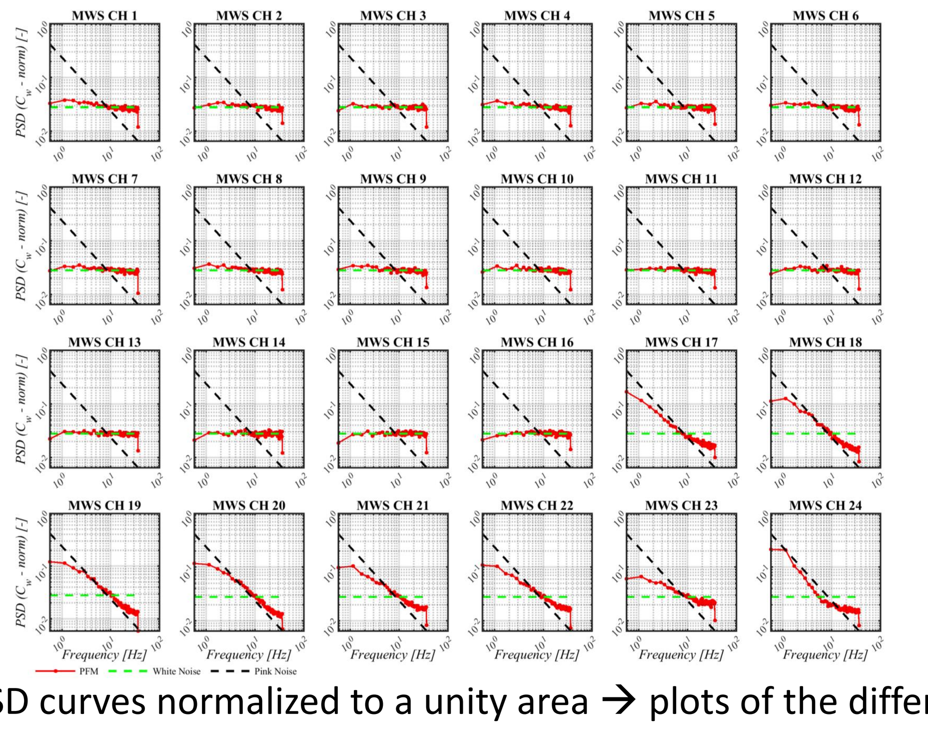

- PSD curves normalized to a unity area → plots of the different channels directly comparable (i.e. removing the dependence range variation of the counts)
- Plots confirm that, up to Channel 16, the noise is almost only white, while for Channel 17 and above the flicker noise dominates.

1.2 Initial radiometric biases

- Shown here: $\Delta T = T_a - ET$ (Antenna temperature minus target temperature) dependency on target temperature, at plateau temperature T2 (consistent with results at T1,T3), no correction applied

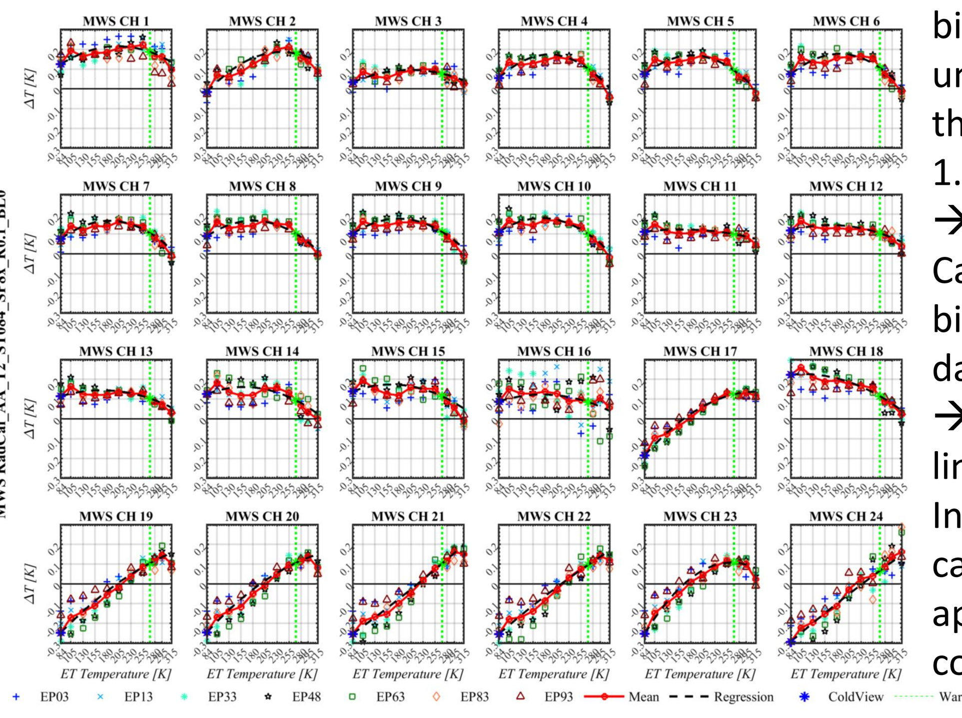

→ Significant cold view bias (impact from non-unity mirror reflectivity of the instrument), see Sec. 1.3

→ Significant On-Board Calibration Target (OBCT) bias at vertical green dashed line, see Sec. 1.4

→ A degree of non-linearity, see Sec. 1.5

In the following, derived calibration parameters are applied sequentially to correct for the biases.

1.3 Mirror-reflectivity

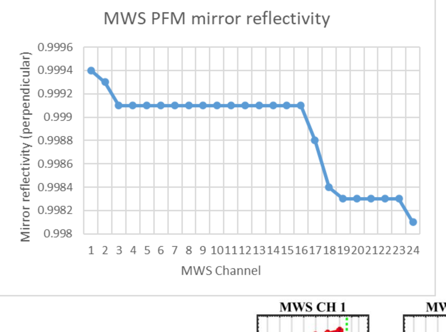

- Red curve: bias ΔT vs ET temperature (as before), using mirror reflectivity=1, without any correction
- Blue curve: bias after applying mirror reflectivity values measured by University Bern [3]

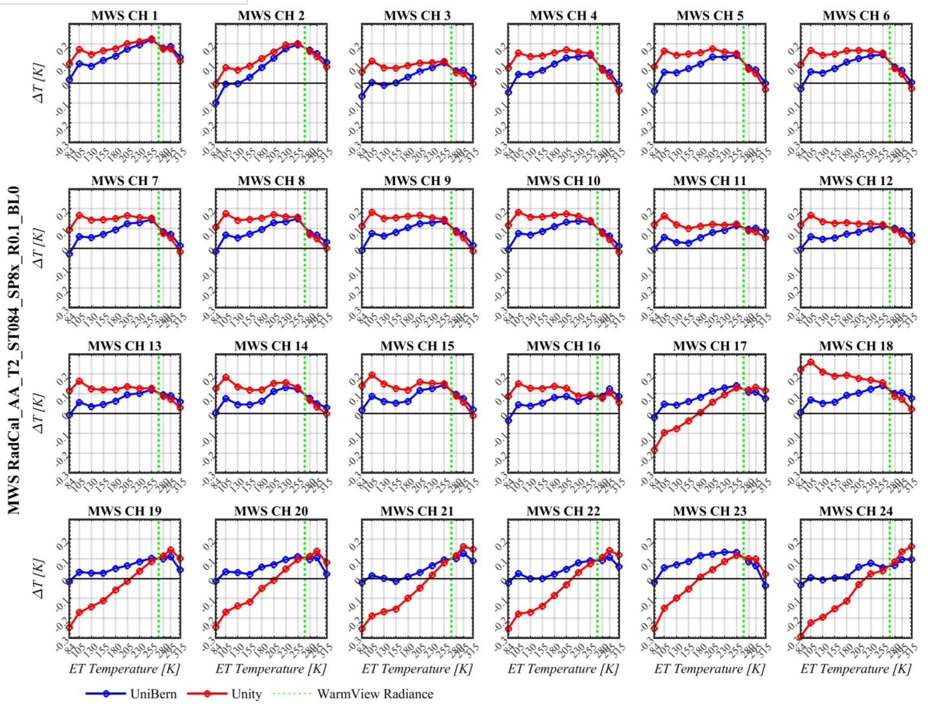

1.4 OBCT correction

- Non-ideal OBCT performance [4]: bias observed at OBCT temp. (at vertical green dashed line in previous plots)
- Correcting for this bias results in the following residual biases, interpreted as non-linearities.

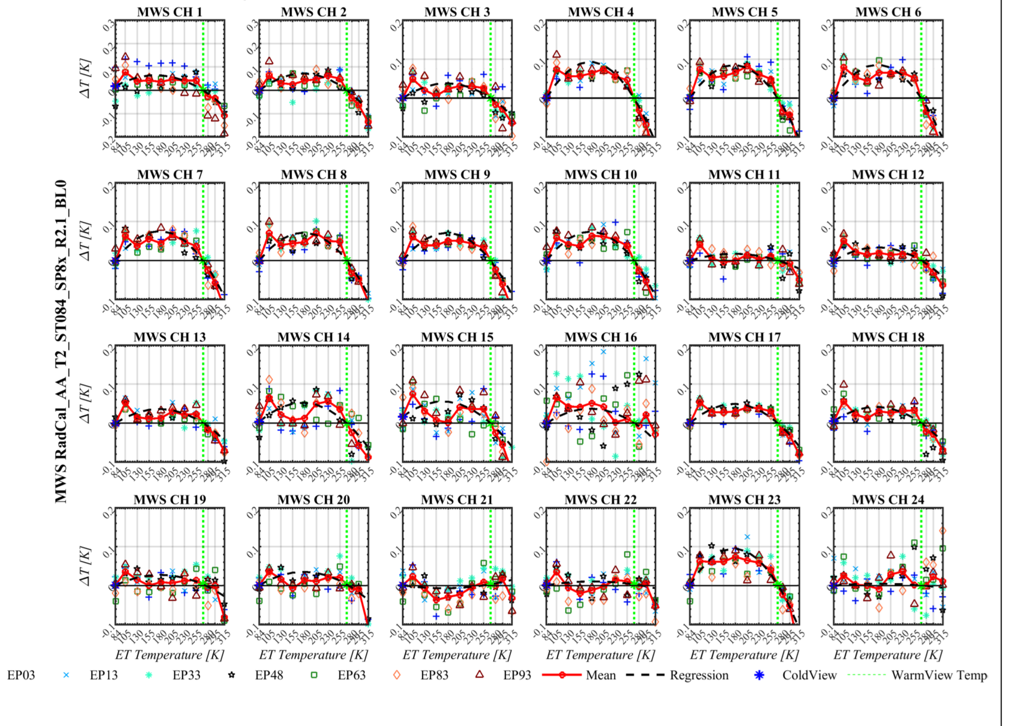

1.5 Non-Linearity

- Nonlinearity parameter μ for plateau temperatures T1,T2,T3 determined from quadratic fit to residuals (previous plot). Note different scale for CH1 and CH2.

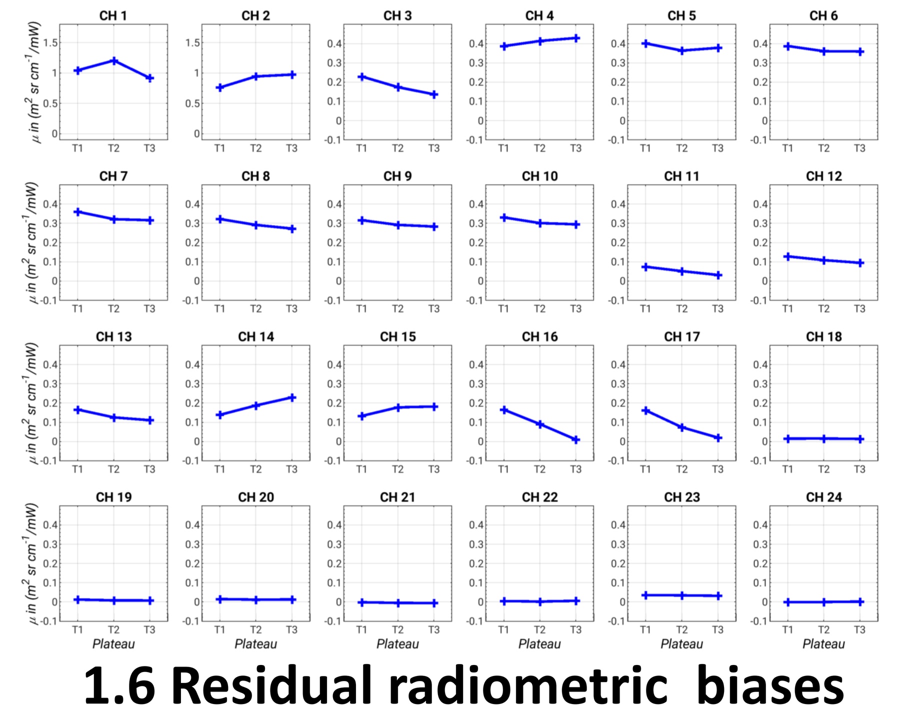

1.6 Residual radiometric biases

- Actual non-unity mirror reflectivity, OBCT correction and non-linearity parameter applied

→ the expected *final residual biases* of retrieved L1B Earth view brightness temperatures are below 0.1K

2. Antenna characterization

- Input: Antenna patterns from industry (fused measurements and simulations)

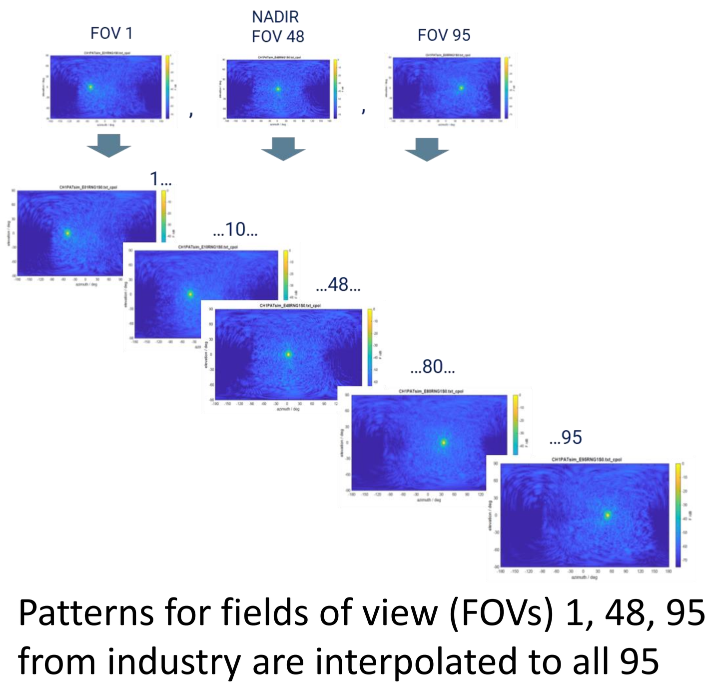

- Patterns for fields of view (FOVs) 1, 48, 95 from industry are interpolated to all 95 FOVs and shifted to correct main beam position per FOV

Beam characterization per FOV:

- Main/ wide beam efficiency: >95%/ >98%
- Beam width: ~1.1° (higher freq. CH) to 2.7° (lower freq. CH)
- Cross-polarization: <1% (higher freq. CH) < 2.6% (lower freq. CH)

→ In line with results from industry and within requirements.

2.1 Antenna correction

Input: 1) Antenna pattern for all FOVs

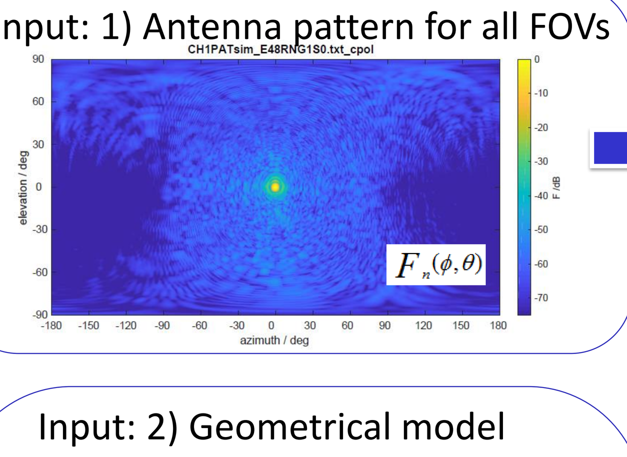

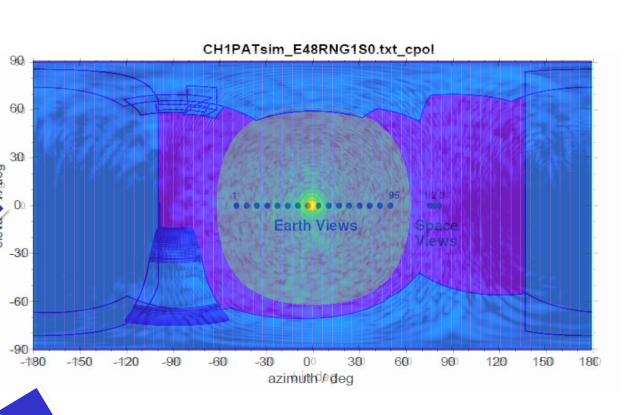

Input: 2) Geometrical model

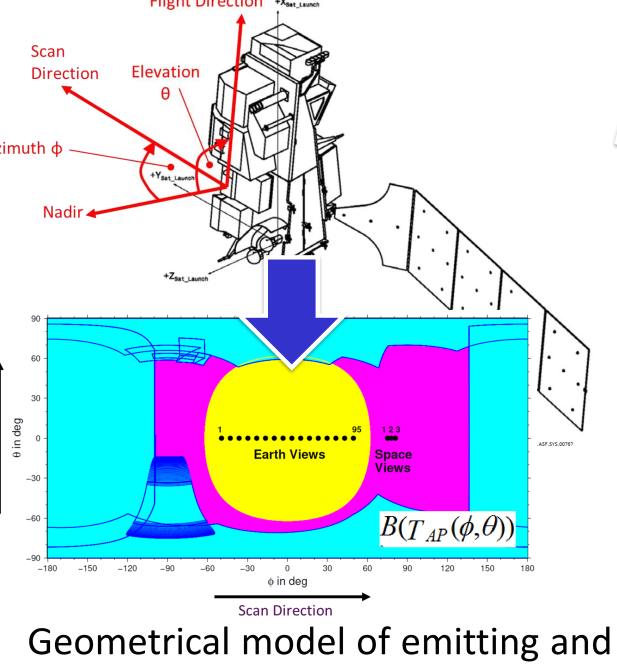

- Geometrical model of emitting and reflecting bodies in the MWS views from Metop-SG geometry.

- Combining information of antenna pattern for all FOVs and geometrical model → antenna efficiencies for Earth, Platform and Space

$$T_A = B^{-1}\left\{\frac{\int_{\phi=\phi_{bor}-90^\circ}^{\phi=\phi_{bor}+90^\circ}\cdot\int_{\theta=-90^\circ}^{\theta=90^\circ} B(T_{AP}(\phi,\theta))\cdot F_n(\phi,\theta)\cdot\cos\theta\cdot d\theta\cdot d\phi}{\Omega_p}\right\}$$

$$\Omega_p = \int_{\phi=\phi_{bor}-90^\circ}^{\phi=\phi_{bor}+90^\circ}\cdot\int_{\theta=-90^\circ}^{\theta=90^\circ} F_n(\phi,\theta)\cdot\cos\theta\cdot d\theta\cdot d\phi$$

$F_n(\phi,\theta) = F_n^{co}(\phi,\theta) + F_n^{cross}(\phi,\theta)$: Antenna Efficiency

θ_{bor} : Boresight Peak Zenith

ϕ_{bor} : Boresight Peak Azimuth

$$T_A = B^{-1}\left\{\begin{array}{l}\eta_E(\phi_{bor},\theta_{bor})\cdot B(T_{APEarth})+\\ \eta_{Sat}(\phi_{bor},\theta_{bor})\cdot B(T_{APSatellite})+\\ \eta_{Space}(\phi_{bor},\theta_{bor})\cdot B(T_{APSpace})\end{array}\right\}$$

$\eta_E, \eta_{Sat}, \eta_{Space}$: Antenna Efficiencies of Earth, Platform, and Space

$T_{APEarth}$: Antenna Corrected Earth View Temperature

$T_{APSatellite}$: Platform Temperature

$T_{APSpace}$: Temperature of Space

B^{-1} : Planck Inverse Operator

2.2 Correction for Earth views

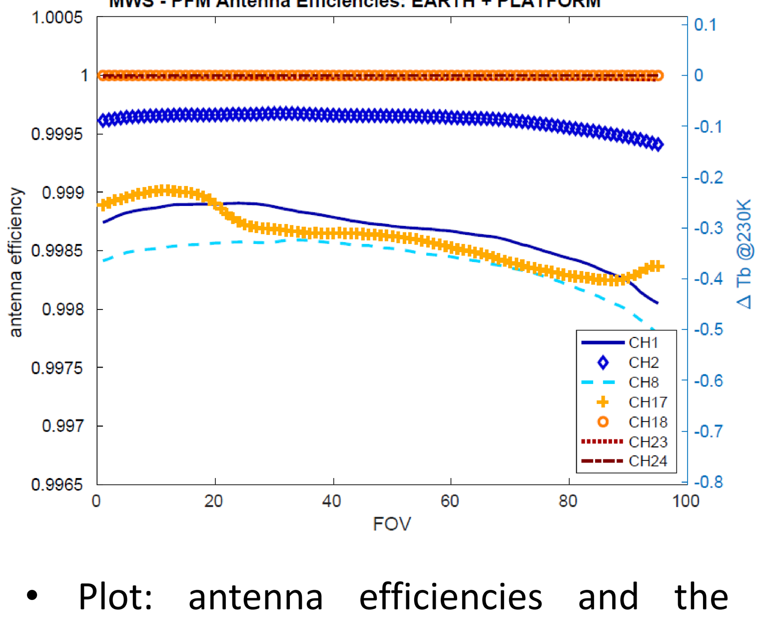

- Plot: antenna efficiencies and the corresponding brightness temperature difference vs. a scene of 230K
- Ideal value = 1 (no side lobe effects)
- Range of numbers and overall shape of curves as expected
- CH17 has a decrease around FOV20 (a side lobe enters space region)
- CH18 hidden behind CH24
- CH18,23,24 have no sidelobes outside the confined region of 10 deg around the main beam.

2.3 Space view correction

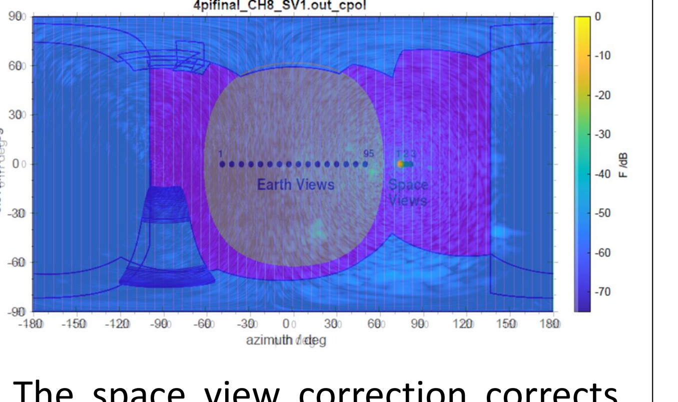

- The space view correction corrects for the impact of Earth (and platform) radiance in the side lobes
- For SV1 (space view) at 75deg, the impact is largest, compared to SV3 at 81 deg.
- Correspondingly the space view correction is largest for SV1 and smallest for SV3

CH	Channel freq. in GHz	SV correction in K at 75°	SV correction in K at 78°	SV correction in K at 81°
1	23	0.79	0.76	0.73
2	31	0.23	0.23	0.22
8	54 main	0.98	0.96	0.93
8	54 red	0.98	0.96	0.94
17	89	0.99	0.98	0.96
18	166	1.47E-04	1.17E-04	9.75E-05
23	183	5.32E-02	5.31E-02	5.34E-02
24	229	3.31E-05	3.31E-05	3.31E-05

3. Summary

- Pre-launch characterization of MWS PFM was comprehensive
- The instrument is expected to perform according to specifications in flight
- Main calibration correction terms have been derived for MWS PFM
  - Mirror reflectivity
  - OBCT correction
  - Non-linearity
  - Antenna pattern correction coefficients

→ Reduce the biases observed in pre-launch RadCal campaign, and correct for impact of side lobes of antenna, respectively

→ Included in CCDB (Calibration Characterization Data Base) auxiliary file for MWS L1B processing

References

- [1] MWS Science Plan, EUMETSAT, 2019, available at https://www.eumetsat.int/science-plans-future-missions
- [2] STFC RAL Space www.ralspace.stfc.ac.uk/Pages/MWS-pfm-installed-on-metop-sg.aspx
- [3] A. Murk, "Reflectivity Measurements of MWS Reflector Samples for MetOP-SG", 2017-04-MW, Microwave Physics Division, Institute of Applied Physics, University Bern
- [4] A. Schröder, A. Murk, R. Wylde, D. Schobert and M. Winser, "Brightness Temperature Computation of Microwave Calibration Targets," in *IEEE Transactions on Geoscience and Remote Sensing*, vol. 55, no. 12, pp. 7104-7112, Dec. 2017, doi: 10.1109/TGRS.2017.2740559.